THE ASTROPHYSICAL JOURNAL, 521:552–560, 1999 August 20

SPECTRAL EVOLUTION OF PKS 2155−304 OBSERVED WITH *BeppoSAX* DURING AN ACTIVE GAMMA-RAY PHASE

L. CHIAPPETTI,[1] L. MARASCHI,[2] F. TAVECCHIO,[2,1] A. CELOTTI,[3] G. FOSSATI,[3] G. GHISELLINI,[2] P. GIOMMI,[4] E. PIAN,[5] G. TAGLIAFERRI,[2] A. TREVES,[6] C. M. URRY,[7] AND Y. H. ZHANG[3]

Received 1998 November 19; accepted 1999 March 30

ABSTRACT

We present the results of *BeppoSAX* observations of PKS 2155−304 during an intense gamma-ray flare. The source was in a high X-ray state. A temporal analysis of the data reveals a tendency of the amplitude of variations to increase with energy and the presence of a soft lag with a timescale of the order 10^3 s. A curved continuum spectrum, with no evidence of spectral features, extends up to ∼50 keV, while there is indication of a flatter component emerging at higher energies, consistent with the interpretation of the broadband spectral energy distribution (SED) due to synchrotron self-Compton emission from a single region. Notably, the fitting of the SED with such a model is consistent with an interpretation of the detected soft lag due to radiative cooling, supporting the idea that radiation losses play an important role in variability. The observed shifts of the SED peaks between the lowest and highest flux levels can be accounted for by an increase of the "break" energy in the relativistic particle spectrum. The model predicts emission at TeV energies in good agreement with the recently reported detection.

Subject headings: BL Lacertae objects: individual (PKS 2155−304) — gamma rays: observations — X-rays: galaxies

1. INTRODUCTION

BL Lacertae objects are a rare class of active galactic nuclei characterized by strong and variable nonthermal emission extending from the radio to the gamma-ray band. The nonthermal continuum is commonly attributed to synchrotron and inverse Compton (IC) radiation emitted in a relativistic jet pointing toward the observer (e.g., Urry & Padovani 1995).

PKS 2155−304 is one of the brightest BL Lacs in the X-ray band and one of the few detected in gamma rays by the EGRET experiment on the *Compton Gamma Ray Observatory* (*CGRO*; Vestrand, Stacy, & Sreekumar 1995). Its broadband spectrum indicates that the radio to X-ray emission is due to synchrotron radiation with a peak in the power per decade distribution between the UV and the soft X-ray band, corresponding to the definition of a high-frequency peak BL Lac (HBL; Padovani & Giommi 1995). The gamma-ray spectrum in the EGRET range (0.1–10 GeV) is flat ($\alpha_\gamma \simeq 0.7$), indicating that the peak of the inverse Compton power is beyond ∼10 GeV. The source has only recently been detected in the TeV band (see below).

In the past years PKS 2155−304 has been the target of numerous multiwavelength campaigns involving observations from the X-rays to longer wavelengths. In the 1994 May campaign (Urry et al. 1997), a well-defined flare was seen in the X-ray band (*ASCA*), followed by less pronounced flares in the *Extreme Ultraviolet Explorer* (*EUVE*) and UV ranges, lagging the X-rays by 1 and 2 days, respectively. A time lag between variations in different X-ray bands (0.5–1 and 2.2–8 keV) was also reported (Makino et al. 1996). In a previous multiwavelength campaign, based on *ROSAT* and *IUE*, correlated low-amplitude fluctuations were observed but no lag larger than a few hours was seen between the X-ray and UV variations (Edelson et al. 1995).

According to the basic scenario, the X-ray emission is due to synchrotron radiation from the highest energy electrons, and the complex spectral variability observed in this band therefore reflects the injection and radiative evolution of freshly accelerated particles.

No observations at other wavelengths simultaneous with one in gamma rays were ever obtained previously for this source, yet it is essential to measure the inverse Compton and synchrotron peaks at the same time in order to unambiguously constrain emission models (e.g., Dermer, Sturner, & Schlickeiser 1997; Tavecchio, Maraschi, & Ghisellini 1998).

For this reason, having been informed by the EGRET team of their observing plan and of the positive results of the first days of the *CGRO* observation, we decided—with the agreement of the *BeppoSAX* time allocation committee and the collaboration of the *BeppoSAX* Science Data Centre (SDC)—to swap a prescheduled target of our *BeppoSAX* blazar program with PKS 2155−304. During 1997 November 11–17 (Sreekumar & Vestrand 1997), the gamma-ray flux from PKS 2155−304 was very high, roughly a factor of 3 greater than the highest flux previously measured from this object. *BeppoSAX* pointed at this source for about 1.5 days beginning 1997 November 22. A quick-look analysis also indicated that the X-ray flux was close to the highest detected level (Chiappetti & Torroni 1997) and higher by a factor of 2 than that observed by *BeppoSAX* in 1996 (Giommi et al. 1998). During the completion of this work, we were informed that the source was detected at TeV energies by the University of Durham TeV telescope Mark 6 (Chadwick et al. 1999) at the time of the *BeppoSAX* observations.

Here we report and discuss the data obtained by *BeppoSAX*. The structure of the paper is as follows: the

[1] Istituto di Fisica Cosmica G. Occhialini, IFCTR/CNR, via Bassini 15, I-20133 Milano, Italy; lucio@ifctr.mi.cnr.it.
[2] Osservatorio Astronomico di Brera, Milano and Merate, Italy.
[3] International School of Advanced Studies, SISSA/ISAS, Trieste, Italy.
[4] *BeppoSAX* Science Data Centre, SDC/ASI, Rome, Italy.
[5] Istituto ITESRE, CNR, Bologna, Italy.
[6] Istituto di Fisica, Università dell'Insubria, Como, Italy.
[7] Space Telescope Science Institute, Baltimore, MD.

relevant information on the observations is given in § 2, and the data analysis methods are presented in detail for each instrument in § 3; light curves and temporal analysis are reported in § 4, while the spectral results are the subject of § 5. Finally, in § 6 the implications for theoretical models are discussed. Conclusions are summarized in § 7.

2. OBSERVATIONS

The *BeppoSAX* scientific payload (see Boella et al. 1997a) includes four Narrow-Field Instruments pointing in the same direction. Namely, there are two imaging instruments: the low-energy concentrator spectrometer (LECS), sensitive in the range 0.1–10 keV (Parmar et al. 1997), and the medium-energy concentrator spectrometer (MECS), sensitive in the range 1.3–10 keV (Boella et al. 1997b) and consisting of three identical units. Both the LECS detector and the three MECS detectors are gas scintillation proportional counters (GSPC) and are in the focus of four identical X-ray telescopes. In addition, there are two collimated instruments: the high-pressure gas scintillation proportional counter (HPGSPC), sensitive in the 4–120 keV range (Manzo et al. 1997), and the phoswich detector system (PDS), sensitive from 12 to 300 keV (Frontera et al. 1997).

BeppoSAX narrow-field instruments observed PKS 2155−304 for slightly less than 1.5 days from 1997 November 22 16:03 UT to 1997 November 24 01:35 UT. The total exposure time was about 22 ks for the LECS and 63 ks for the two MECS units now in operation (M2 and M3), with an average count rate of 0.64 (1.8–10 keV) counts s^{-1} in a single MECS unit (corresponding to about 5 mcrab) and 2.21 counts s^{-1} in the LECS (0.1–4 keV band).

The HPGSPC and PDS were operated in the customary collimator rocking mode, where each collimator points alternately at the source and at the background for 96 s. In the case of the HPGSPC, there is a single collimator, so the whole instrument is looking at the target for half of the time and in the offset negative direction for the other half. The resulting source exposure time was 29 ks, and the source was detected at least up to 30 keV with a rate of 0.5 counts s^{-1}. The PDS has two collimators: at any time one of them looks at the source, and the other one at the background. Therefore, the target is observed continuously (in our case the exposure time was 28 + 29 = 57 ks), but using only half of the collecting area, with a count rate between 0.2 and 0.3 counts s^{-1}.

3. DATA REDUCTION

The data reduction for MECS, PDS, and HPGSPC was done using the XAS software (Chiappetti & Dal Fiume 1997) on telemetry files contained in the Final Observation Tapes. For the LECS, we have used the linearized, cleaned event files version rev. 1.0 generated at the *BeppoSAX* SDC.

We have preliminarily selected the intervals in which the satellite was pointing at the source (unocculted by Earth, i.e., Earth elevation angle greater than 3°) using the information in the attitude files. In addition, for collimated instruments we have excluded the first 5 minutes after egress from the South Atlantic Geomagnetic Anomaly, when the instrument gain is being calibrated.

3.1. *Imaging Instruments*

As part of the standard data accumulation for both LECS and MECS, a number of corrections are applied to each photon, namely, the positional coordinates are linearized (correcting for geometrical distortion) and the energy of each photon is referred to the detector center (compensating for known spatial disuniformities of gain) and corrected to a standard gain using the gain histories to remove the temperature dependency of gain. In our case, we verified the stability of the gain within at worst 2% during the initial orbits.

For both instruments the preferred background subtraction method is to use a background spectrum accumulated from blank field exposures in the *same* detector region where the target spectrum is accumulated. The accumulation of a simultaneous background spectrum in a *surrounding* annulus would instead include a residual contribution from the target. In fact, an extraction radius of the order of 8′, as used here, leaves out ∼2%–4% of the point-spread function, depending on energy.

3.1.1. *MECS*

Source spectra and light curves were accumulated in a circular region of 8.′4 radius around the target position. In order to improve particle background rejection, we also applied burst length thresholds (channels 25–55 for M2, and 27–60 for M3) consistent with the standard response matrices.

The background was accumulated in the same region from a large data set of blank fields obtained during the *BeppoSAX* performance verification (PV) phase (and available to IFCTR as a *BeppoSAX* hardware institute) for a total exposure time of 1120 ks. In addition to the considerations made above, in the case of the MECS this must also be preferred because the outermost part of the field of view is known to be affected by residual contamination from misplaced calibration events (Chiappetti et al. 1998).

3.1.2. *LECS*

The LECS data analysis was based on the cleaned and linearized event files processed at the SDC. The events were extracted with XSELECT within a circle centered on the source radius of 8.′5. Since the count rate of the source is very high, the background is not very important, and we used the standard background files supplied by SDC. The spectral analysis was performed using the calibrations released in 1997 September.

3.2. *Collimated Instruments*

3.2.1. *PDS*

The standard PDS spectra accumulation occurs via the following procedure. One first creates the time profiles of both collimator positions (sampled at 1 s resolution) and generates for each three sets of time windows, corresponding to stable positions on-source and offset in the positive (off +) and negative (off −) directions. Then three spectra in raw PHA channels for each unit are accumulated over the respective time windows (background + source, and background in the off + and off − cases).

A merged background spectrum for each unit (exposure-weighted sum of the off + and off − spectra) is then generated and subtracted from the on-source spectrum. In order to sum the net spectra of the four units, one must equalize the respective gain (i.e., convert from PHA channels to keV using unit-specific relations assuming a standard gain), which is done contextually with a user-selected rebinning (usually logarithmic) in energy space.

During accumulation one also applies a default rise time threshold (channels 3–150) to improve rejection of non–X-ray events. For medium-weak sources, one can apply an additional set of narrower energy-dependent rise time thresholds (so-called PSA correction method). The rise time of individual photons is compensated for temperature variations with respect to the nominal temperature for which the thresholds have been generated. In this way a 40% reduction of the background is achieved (from 10 to 6 counts s^{-1}), with a smaller effect on the net rate (which is accounted for by a 10%–20% adjustment of the cross normalization of the PDS response matrix with respect to the MECS one): in our case we obtain on the overall energy range 0.27 ± 0.05 counts s^{-1} (no correction) and 0.21 ± 0.03 counts s^{-1} (with correction), which are consistent within the errors.

We verified the quality of the background subtraction by subtracting the off+ and off− raw background spectra of each unit from each other, and then summing the difference spectra of the four units exactly in the same way described above for the production of net spectra. Indeed the resulting signal (0.06 ± 0.06 counts s^{-1}) is consistent with zero.

PDS data may be affected by spurious spikes due to the *fluctuations* of metastable phosphorescence induced in the crystals by particles, interpreted by the electronics as spikes in the count rate (as high as 300 counts in a 0.1 s interval). A spike filtering has been applied to all spectra and light curves, rejecting all time intervals where the scientific data rate (in the PHA range 10–350, and in the rise time range 3–130) is above 25 counts s^{-1}.

Since the signal is weak, we have not attempted to accumulate binned light curves. Similar to MECS and HPGSPC, we used instead large bins of variable size (of the order of 1 hr or less) corresponding to unocculted intervals in each orbit, and we accumulated three separate light curves for each PDS unit (for the on-source, off+, and off− cases, taking into account the exposure fraction of each bin), made a weighted combination of the off+ and off− curves, subtracted it from the source+background one, and finally summed the four unit net curves.

3.2.2. *HPGSPC*

The standard HPGSPC spectra accumulation is similar to the procedure described above for the PDS. However, one has only one collimator position time profile and just two disjoint time windows, corresponding to stable positions on-source and offset in the negative directions. Then one accumulates two spectra over the respective time windows (background+source and offset background), also applying the burst length thresholds (channels 80–115) to improve rejection of non–X-ray events. The background must be corrected before subtraction by adding a difference spectrum, which compensates for effects due to the different position of the collimators (mainly the illumination by the calibration sources).

As for the PDS, we used "coarse variable bins," as defined above, to generate light curves for the on-source and offset cases. We subtracted the uncorrected background plus a further constant, corresponding to the integral of the difference spectrum in the wished PHA channel range. We intended to "hook up" our HPGSPC data with MECS and PDS data in the overlapping energy ranges. However, the HPGSPC 5–10 keV curve shows excesses with respect to the MECS in a couple of orbits, related to ^{55}Fe calibration events not rejected properly by the onboard tagging. Further occasional deviations still present in the 7–10 keV range suggest that the stability of the difference spectra with time is poorly known, throwing doubts also on the confidence of HPGSPC 10–16 keV light curves.

4. RESULTS

4.1. *Light Curves*

In Figure 1 we show the MECS light curve at 120 s resolution. Epochs of high, low, and intermediate intensity, which will be used to integrate spectra at different intensity levels, are indicated with letters A–F (see § 4.2). In Figure 2 (*top panels*), we show the light curves binned over 1000 s in different energy bands: 0.1–2 keV for the LECS, and 2–4 keV and 4–10 keV for the MECS. The source reaches a peak after the first 2 hr of observation (A in Fig. 1) and declines by a factor of 3 (maximum/minimum) in the following 10 hr. A smaller flare (D in Fig. 1) follows, and the light curve seems to stabilize in the interval indicated as F. The variability timescale appears to be well resolved, and no episode of very fast variability ($Fdt/dF < 1h$) is apparent.

The most rapid variation observed (the decline from the peak at the start of the observation) has a halving timescale of about 2×10^4 s, similar to previous occasions (see, e.g., Urry et al. 1997). Light curves from the higher energy instruments were derived as detailed in § 2, but no significant variability was detected because of poor statistics.

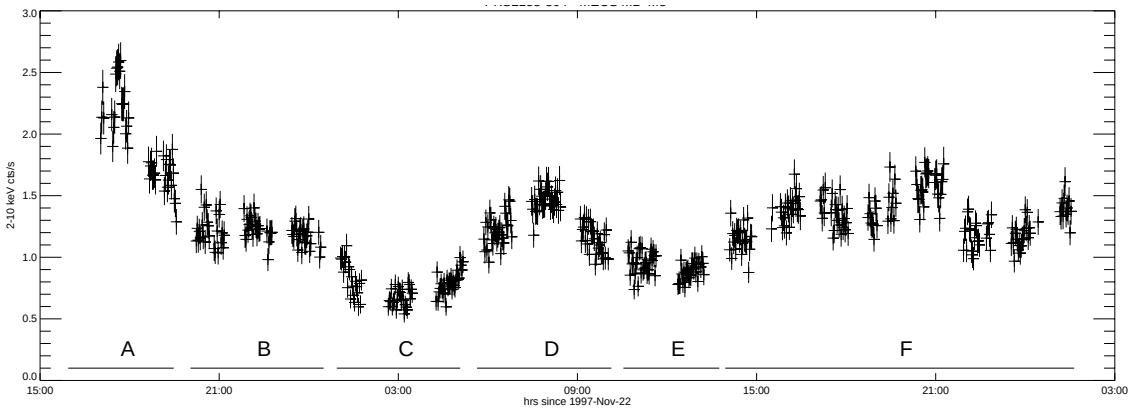

FIG. 1.—MECS light curve at 120 s resolution. As described in the text, the spectral analysis has also been performed in separate time intervals, indicated as A–F in the figure.

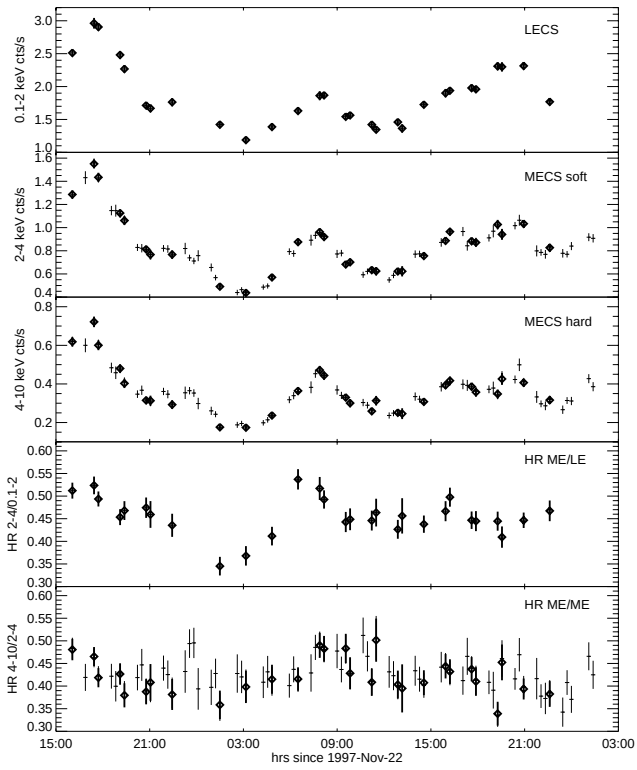

FIG. 2.—Light curves and hardness ratios for different energy bands in 1000 s bins. In the top three panels we show the light curves in the 0.1–1 keV, 2–4 keV, and 4–10 keV energy bands, respectively, while the bottom two panels show the 2–4/0.1–2 and 4–10/2–4 ratios. Note that the coverage of the LECS is more limited than the one of the MECS, because the LECS is operated only during dark times in order to avoid UV light contamination through the entrance window. The points simultaneous with the presence of LECS data are indicated as diamonds. The 2–4/0.1–2 hardness ratio shows a clear correlation with the source intensity.

The variability amplitude is different in the three bands, increasing with increasing energy. In order to characterize this energy dependence better, hardness ratios between the 2–4/0.1–2 keV (HR1) and the 4–10/2–4 keV (HR2) bands were computed. They are shown in the lower panels of Figure 2. HR1 has smaller uncertainties and clearly increases with intensity in a correlated fashion on the timescale of each peak. However, the correlation is not biunivocal: HR1 has the same value at the first two peaks (A and D), which have significantly different intensities, and is lower toward the end of the observation when the average intensity is similar to that of peak D. Note also that for both the first and the second peak the hardness ratio is high already before the peak is reached. HR2 does not show a clear trend, which could be because of the larger uncertainties and the smaller energy range. The issue of spectral variability is further discussed below (§ 4.2.3).

We looked for time lags between variations at different energies as suggested by the *ASCA* observations of this same source and of Mrk 421 (Makino et al. 1996; Takahashi et al. 1996). The presence of a soft lag is indicated by the fact that the hardness ratio increases *before* the intensity peaks, as is the case in our light curve.

To quantify the lag we used the discrete correlation function method developed by Edelson & Krolik (1988) for data sets with irregular spacings. We binned the light curves in smaller and smaller bins since no lag was apparent for bin sizes larger than 1000 s. In Figure 3 we show the discrete

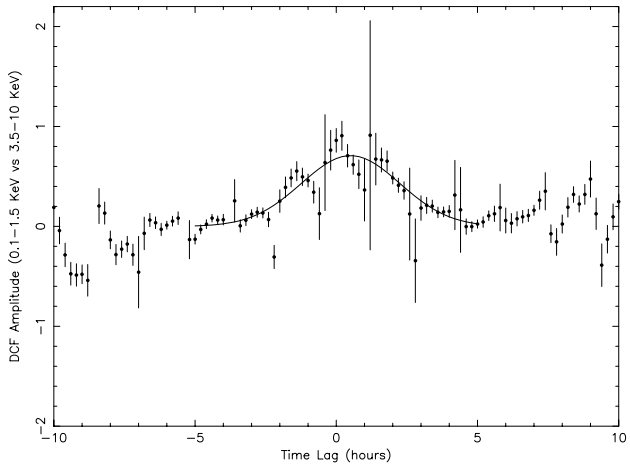

FIG. 3.—Discrete correlation function between the 0.1–1.5 keV and 3.5–10 keV light curves (binned in 300 s intervals, using a discrete correlation function bin size of 0.2 hr) together with its Gaussian fit. A positive lag indicates that the high-energy X-rays lead the low-energy ones.

correlation function obtained correlating the light curves in the bands 0.1–1.5 (LECS) and 3.5–10 keV (MECS). A Gaussian fit, which takes into account the overall symmetry of the distribution around the peak, yields a maximum corresponding to a soft lag of 0.50 hr (with a 1 σ error of 0.08 hr). We also applied the minimum mean deviation method (Hufnagel & Bregman 1992; Fig. 4). Here the correlation estimator is the mean deviation of the two cross-correlated light curves: the minimum mean deviation corresponds to the best cross correlation. A Gaussian fit to this minimum again gives a soft lag of 0.33 ± 0.07 hr.

The issue of the lags and their uncertainties, estimated with a Monte Carlo procedure, is discussed in detail in Treves et al. (1998) and Zhang et al. (1999), where a comparison is made with the 1996 *BeppoSAX* (Giommi et al. 1998) and 1994 *ASCA* data (Makino et al. 1996).

4.2. *Spectra*

We analyzed the overall spectrum first from the entire observation separately for each instrument and then by combining different instruments. We also studied spectral variability, accumulating spectra in the time intervals indi-

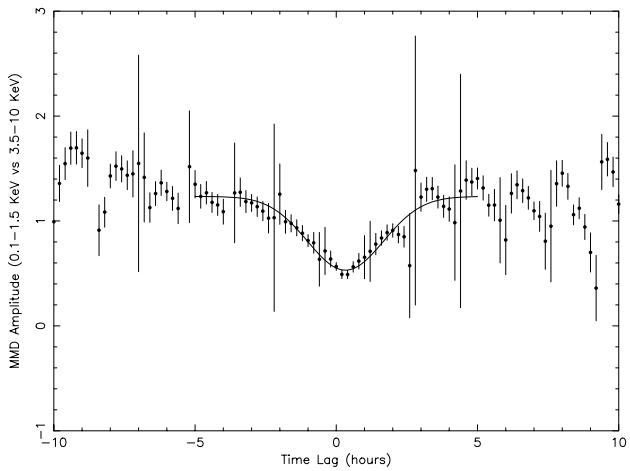

FIG. 4.—Minimum mean deviation for the same light curves and with the same conventions used in Fig. 3, with its own Gaussian fit.

cated as A–F in Figure 1. When not differently stated, we used in the fits the value of the galactic column density reported by Lockman & Savage (1995), $N_{\rm H} = 1.36 \times 10^{20}$ cm^{-2}.

For the spectral fitting procedures, the LECS and MECS data were binned in energy according to the template provided by SDC,[8] which takes into account the effective energy resolution of the spectrometers. For the high-energy instrument, data have been severely rebinned as described below. In all cases we considered for the LECS the energy range 0.1–4 keV, and for the MECS the range 2–10 keV.

The response matrices are generated according to the accumulation conditions (extraction radius, binning, etc.) for the MECS and PDS case using the latest version of the XAS software, while for LECS and HPGSPC case standard matrices are used, as released in 1997 September (with optional rebinning). Results of the fits are summarized in Table 1.

4.2.1. *Single Instruments*

LECS.—A single power law is a poor fit to the LECS data, although it yields an $N_{\rm H}$ value quite close to the galactic one. An acceptable fit is obtained by modeling the spectrum with a broken power law (see Table 1); in the latter case, also, the $N_{\rm H}$ determined by the fit is consistent with the galactic one, which was therefore fixed in all of the following fits. The residuals of this fit do not show clear evidence of spectral features in absorption or emission. In particular, we do not detect absorption near 0.6 keV as seen in some previous observations (Canizares & Kruper 1984; Madejski et al. 1991; see, however, Brinkmann et al. 1994).

MECS.—The MECS alone is not sensitive to low values of $N_{\rm H}$ because of the low-energy cutoff induced by the beryllium window. A fit with a single power law and free column density gives χ^2 close to unity but yields an ill-determined $N_{\rm H}$ of several 10^{21} cm^{-2}, inconsistent with the results from the LECS. When fixing $N_{\rm H}$ to the galactic value, a broken power-law model describes well the spectrum within the 2–10 keV band (see Table 1). Note that the spectral index in the higher energy range of the LECS (1–4 keV) is similar to that in the lower energy range of the MECS (2–3 keV), giving us confidence that the increasing slope suggested by the fits is a good representation of the spectrum.

HPGSPC.—The HPGSPC data were rebinned ad hoc into 8 bins. The signal is present very clearly (greater than 4 σ) up to 13 keV and with a lower statistical significance up to at least 24 keV (i.e., below the Xe K edge). As MECS and HPGSPC are very well cross-calibrated (Cusumano et al. 1999), and since this spectrum lies well on the extrapolation of the MECS fit, it has been fitted only in combination with spectra from other instruments.

PDS.—For the PDS we used a very coarse grouping in just four logarithmic bins. The signal from the source is clearly visible in the first bin (up to 26 keV) and remains present at a nonzero level (although with a poorer significance, $\simeq 2\ \sigma$) in the other bins. Fitting the PDS data with a single power law yields a poor result, with a spectral index *flatter* than in the MECS band.

4.2.2. *Combined Spectra*

We fitted the composite LECS + MECS spectrum over the entire range 0.1–10.5 keV (see Table 1). Given that the single-instrument spectra are well described by broken power-law models, we tried to reproduce the composite spectrum with the same model. We allowed for a free relative normalization between the LECS and MECS data, and the best-fit value found (LECS norm/ MECS norm $\simeq 0.7$) is consistent with previous works. However, the fit is unacceptable. In Figure 5 we show the results of the fitting procedure: the model does not represent the data well ($\chi^2_{\rm red} = 2.3$), and the shape of the residuals indicates that the spec-

[8] For more information on the template and spectral fitting procedures, see Fiore & M. Guainazzi 1997, SAX Scientific Analysis Cookbook: Spectral Analysis, available on the World Wide Web at http://www.sdc.asi.it/software/cookbook/spectral.html.

TABLE 1

BEST-FIT PARAMETERS

Data Set	$N_{\rm H}$ [a]	Γ [b]	χ^2/dof [b]	Γ_1 [c]	Γ_2 [c]	E_b (keV) [c]	χ^2/dof [c]	Flux [d]
LECS, all	$2.1^{+0.1}_{-0.05}$	2.38 ± 0.02	207/48	...	...	...	...	...
	1.4 ± 0.1	...	...	2.09 ± 0.05	2.54 ± 0.04	1.1 ± 0.1	56.4/45	...
	1.36 (fix)	2.21 ± 0.01	57.4/48	2.06 ± 0.02	2.54 ± 0.04	1.1 ± 0.1	57.4/47	...
MECS, all	41 ± 20	2.92 ± 0.04	74.1/56	...	...	...	...	...
	1.36 (fix)	2.78 ± 0.02	118/57	$2.64^{+0.06}_{-0.08}$	$2.88^{+0.07}_{-0.03}$	3.2 ± 0.1	76.2/55	...
PDS, all	...	$2.1^{+1.7}_{-0.8}$	5.0/2	...	...	...	...	...
LECS + MECS, all	1.36 (fix)	...	...	2.09 ± 0.02	2.76 ± 0.02	1.4 ± 0.1	244.0/105	...
MECS + PDS, all	1.36 (fix)	...	...	$2.65^{+0.05}_{-0.09}$	2.90 ± 0.05	3.2 ± 0.1	87.2/58	...
MECS + HPGSPC + PDS, all	1.36 (fix)	...	...	$2.65^{+0.05}_{-0.08}$	2.89 ± 0.04	3.2 ± 0.1	85.8/64	...
LECS + MECS, all	1.36 (fix)	...	...	2.07 ± 0.02	2.63 ± 0.03	1.2 ± 0.1	153.4/103	0.81
				2.63 (fix)	2.90 ± 0.04	3.3 ± 0.2		
LECS + MECS, A	1.36 (fix)	...	...	2.00 ± 0.04	2.57 ± 0.07	1.2 ± 0.2	145.3/102	1.27
				2.57 (fix)	2.97 ± 0.12	3.5 ± 0.5		
LECS + MECS, B + D + F	1.36 (fix)	...	...	2.08 ± 0.02	2.66 ± 0.03	1.2 ± 0.1	130.8/103	0.85
				2.66 (fix)	2.90 ± 0.05	3.2 ± 0.3		
LECS + MECS, C + E	1.36 (fix)	...	...	2.15 ± 0.05	2.61 ± 0.09	1.1 ± 0.1	92.7/102	0.54
				2.61 (fix)	2.89 ± 0.07	2.9 ± 0.2		

NOTE.—All errors quoted are at 90% confidence level.

[a] 10^{20} cm^{-2}.

[b] Single power-law model.

[c] Broken power-law model.

[d] Flux at the source in the 2–10 keV band, in 10^{-10} ergs cm^{-2} s^{-1}.

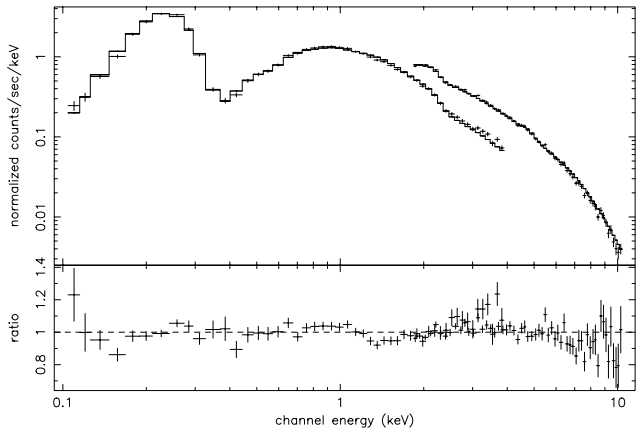

FIG. 5.—LECS+MECS spectra fitted with the broken power-law model (see Table 1).

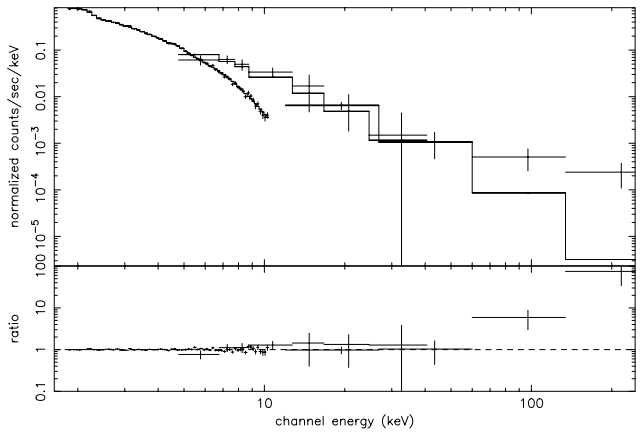

FIG. 6.—MECS+HPGSPC+PDS spectra fitted with a single broken power law. Note the logarithmic scale for the data/fit ratio.

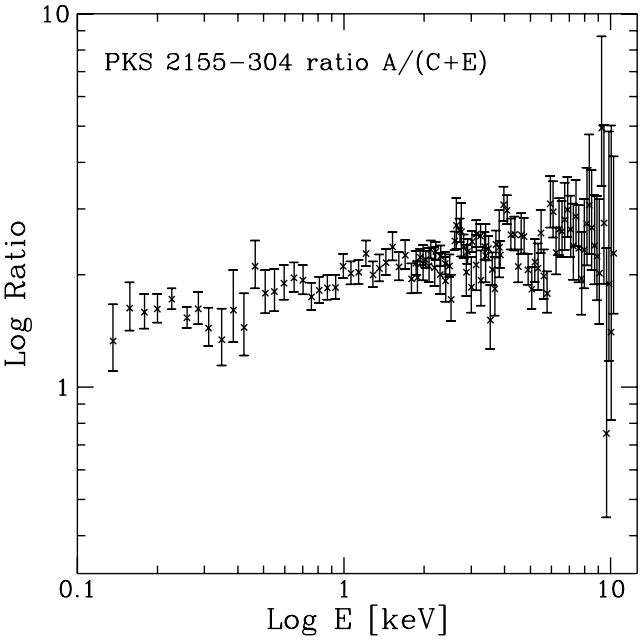

FIG. 7.—Ratio between the flaring state spectrum (A) and the quiescent spectrum (states C and E). The plot shows that the spectrum hardens during the flare, but the estimated variation in the spectral index is very small.

trum is flatter than the model at the lowest energies and steeper at the highest ones. Thus a model describing a more continuous steepening is required, in agreement with the results of the fits to individual spectra, which yield at least two "break" energies (at ~ 1.2 and ~ 3.2 keV, respectively) with spectral indices $\Gamma \sim 2.1$, 2.6, and 2.9. This trend was also found (for this same source) by Giommi et al. (1998), who indeed showed that a good fit can be obtained using a curved model.

Fitting together the MECS and PDS data yields spectral parameters very similar to those obtained for the MECS alone. A cross normalization of 0.8 was used. The residuals show that the PDS data are consistent with an extrapolation of the MECS fit up to about 50 keV. Above this energy the PDS data present a marginal hint of an excess, suggesting—as already found for the PDS alone—a flattening of the spectrum.

Adding also the HPGSPC spectrum to the data set and fitting all three instruments again gives results similar to those obtained for the MECS alone (Fig. 6). Additionally, if one uses MECS data above the 3.2 keV break together with HPGSPC data, they are compatible ($\chi^2 = 55$ for 49 dof) with a broken power-law model with the first spectral index Γ_1 fixed to the value ~ 2.9 derived from the MECS fit, a break around 10 keV, and a flatter slope $\Gamma_2 \sim 2.2$ (no formal simultaneous fit of the break energy and Γ_2 is possible). This is a further element in favor of a flattening of the spectrum at high energies.

4.2.3. *Spectral Variability*

In view of a discussion on spectral variability, the overall observation period has been divided into smaller intervals (indicated as A–F in Fig. 1) using the following approximate intensity windows (referred to a single MECS unit): peak, above 0.8 counts s^{-1} (interval A); intermediate (intervals B, D, and F); dip, below 0.5 counts s^{-1} (intervals C and E). We have then accumulated spectra with the standard prescriptions described above for each interval, and also for the combinations B+D+F and C+E. Additionally, we have divided interval D into two parts ("rise" and "fall") and taken the ratio of the relevant spectra, which has been found to be consistent with unity.

In order to have a model-independent description of the spectral variability, we have computed the spectral ratio between the flaring (A) and the lowest states (C and E). The result is plotted in Figure 7: the ratio continuously increases with energy, yielding clear evidence that the flaring state is harder than the low state. Since this ratio varies by a factor of about 2 over 2 decades, the associated change in the spectral index can be estimated as only $\Delta\alpha \simeq 0.15$.

Both the LECS and MECS spectra for the high, intermediate, and low states were separately fitted with broken power laws, fixing the value of Γ_1 for the MECS fit at the value of Γ_2 obtained from the LECS. The results are reported in Table 1. They are consistent with a hardening of the spectrum with increasing intensity, but the magnitude of this variation is small, as estimated above, comparable with the errors in the fit parameters.

5. BROADBAND SPECTRAL ENERGY DISTRIBUTIONS

In order to estimate the physical parameters of the emitting region, we constructed broadband spectral energy distributions (SED) based on the deconvolved LECS and MECS *BeppoSAX* data at *maximum* and *minimum* intensity

during the present observation (Fig. 8). At higher energies, the PDS data represent averages over the whole *BeppoSAX* observation period. At gamma-ray energies, the EGRET spectrum is plotted as from the discovery observation (Vestrand et al. 1995) and also with an intensity multiplied by a factor of 3 to represent the gamma-ray state of 1997 November 11–17, as communicated by Sreekumar & Vestrand (1997). The *BeppoSAX* observation occurred near the end of the 2 week *CGRO* observation, while the high gamma-ray state was recorded during the first days. In the absence of a gamma-ray flux exactly simultaneous with the *BeppoSAX* data, we consider the two sets of gamma-ray intensities as encompassing the actual values.

At UV wavelengths we plot the maximum and minimum fluxes observed with *IUE* (Edelson et al. 1992; Urry et al. 1993; Pian et al. 1997) and at other wavelengths the maxima and minima as observed during the 1991 and 1994 multiwavelength campaigns (Courvoisier et al. 1995; Pesce et al. 1997).

The shape of the SED can be interpreted as due to two components: the first one, peaking in the soft X-ray range, is commonly attributed to synchrotron radiation, while the second, peaking above 10 GeV as suggested by the flat gamma-ray spectrum, can be accounted for by inverse Compton scattering of the synchrotron photons off the high-energy electrons that produced them, namely the synchrotron self-Compton process (SSC; e.g., Ulrich, Maraschi, & Urry 1997, and references therein).

A simple version of this model considers emission from a homogeneous spherical region of radius R, whose motion can be characterized by a Doppler factor δ, filled with a magnetic field $\boldsymbol{B}$ and with relativistic particles whose energy distribution is described by a broken power law (the latter corresponds to four parameters: two indices n_1, n_2, a break energy $\gamma_b mc^2$, and K, a normalization constant). As discussed in detail by Tavecchio et al. (1998), the seven model parameters listed above can be strongly constrained by using seven observational quantities, namely, the two spectral slopes (in the X- and gamma-ray bands), the frequency and flux of the synchrotron peak, a flux value for the inverse Compton component emission, and a lower limit to the inverse Compton peak frequency. Assuming $R = ct_{\rm var}$ with a variability timescale $t_{\rm var} = 2$ hr, the system is practically closed and we obtain *univocally* a set of physical parameters for the source, with uncertainties depending on those of the observed quantities involved.

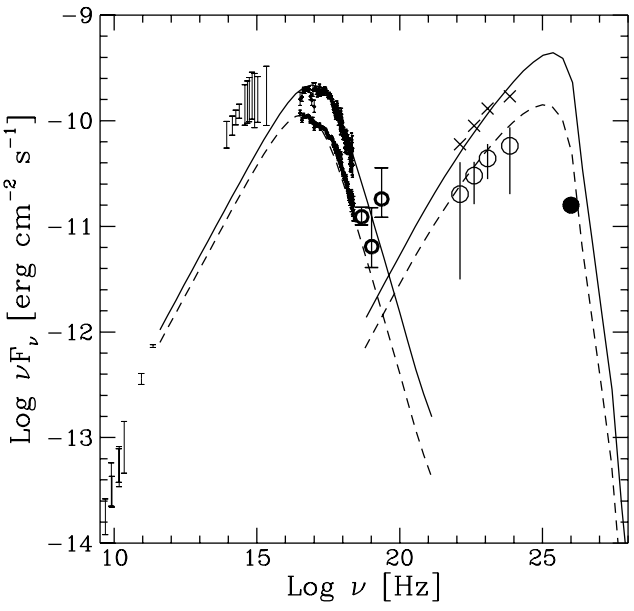

FIG. 8.—SED of PKS 2155−304 with the fit obtained with the SSC homogeneous model in the high (*solid line*) and low (*dashed line*) states. The parameters of the model are reported in the text. The X-ray points (*error bars*) represent the spectra in the high (interval A) and low (intervals C+E) states. The heavy circles corresponding to the PDS points refer to the average spectrum. The circles are EGRET gamma-ray data from Vestrand et al. (1995), and they are also shown (*crosses*) multiplied by a factor of 3 to reproduce the gamma-ray state of 1997 November. The TeV observation (from Chadwick et al. 1999) is also shown (*filled circle*). The vertical bars encompass the range between the minimum and maximum value in a compilation of radio, optical, and UV data (see text for references).

Figure 4 of Tavecchio et al. (1998) shows the allowed region in the $\boldsymbol{B} - \delta$ space derived for PKS 2155−304 with values of the observational quantities encompassing those derived here. A lower limit $\delta > 15$ is set by the "internal" transparency condition for TeV gamma rays, while the limits derived from the modeling of the SED fall somewhat above this.

In Figure 8 we show two SEDs computed with the SSC models described above aimed at reproducing the high and low X-ray states observed with *BeppoSAX*. We (arbitrarily) assumed that the lower intensity X-ray state corresponds to the gamma-ray emission reported in 1995. The parameters of the model for the lower state have the following values: $\delta = 18$, $\boldsymbol{B} = 1$ G, $R = 3 \times 10^{15}$ cm, $n_1 = 2$, $n_2 = 4.85$, $K = 10^{4.7}$, and $\gamma_b = 10^{4.5}$. The inverse Compton emission is computed here with the usual step approximation for the Klein-Nishina cross section, i.e., $\sigma = \sigma_{\rm T}$ for $\gamma v_t < mc^2/h$ and $\sigma = 0$ otherwise, where γ is the Lorentz factor of the electron and v_t is the frequency of the target photon.

The comparison of the flaring spectrum with the lower intensity one in Figure 8 shows that the *peak* in the SED shifted to higher energies during the flare. In fact, the peak occurs at about 1 keV during the flare, while in the fainter states it falls toward the lower end of the *BeppoSAX* range ($\simeq$0.2 keV). A similar behavior was observed in Mrk 421 with *ASCA* (Takahashi et al. 1996) and with *BeppoSAX* (Fossati et al. 1998). A much more extreme case occurred in Mrk 501, when in a state of exceptional activity the SED peak was observed to be in the 100 keV range (Pian et al. 1998).

Therefore, in the model for the flaring state the break energy of the electron spectrum was shifted to higher energies ($K = 10^{4.8}$, $\gamma_b = 10^{4.65}$), leaving the other parameters unchanged. Correspondingly, the inverse Compton peak also increased in flux and moved to higher energies. Both effects are, however, reduced with respect to the "quadratic" relation expected in the Thomson limit, since for the required very high energy electrons the suppression due to the Klein-Nishina regime plays an important role.

The models predict TeV emission at a detectable level. Indeed, toward the completion of this work we were informed of the detection of high-energy gamma rays by the Mark 6 telescope (Chadwick et al. 1999). Part of the Mark 6 observing period overlaps that of *BeppoSAX* and EGRET. Although the exact flux level simultaneous to the *BeppoSAX* one has not been reported, in 1997 November the source was seen by the Mark 6 telescope at its highest flux (Chadwick et al. 1999). The time-averaged flux corresponds to 4.2×10^{-11} photons cm^{-2} s^{-1} above 300 GeV (and extending up to greater than 3 TeV).

Indeed, the model for the lower intensity state reproduces the average TeV emission flux level remarkably well. A more detailed test comparing the TeV fluxes associated with different X-ray states will hopefully be possible with future observations.

Current models of the IR background (Malkan & Stecker 1998) predict an optical depth between 1 and 2 for a 1 TeV photon from a source located at $z \sim 1$ (Stecker & de Jager 1998). The resulting flux reduction would still be consistent with our model. Signatures of this effect may be found in the future from a measurement of the TeV spectral shape.

Note that given the flat soft X-ray spectrum, it would be impossible to reproduce with these same models the non-simultaneous optical UV data reported in the figure. Since the variations occur on longer timescales in the lower energy bands, the optical UV flux may derive from a larger spatial region, which acts as a reservoir for the partially cooled particles. At higher energies instead we may observe the radiation from the freshly accelerated particles before they can accumulate in the reservoir. In this case, a single homogeneous region is not sufficient to describe the full broadband SED. Alternatively, a more complex spectral shape for the electron energy distribution must be assumed.

6. SPECTRAL DYNAMICS

The time-resolved continuum spectroscopy, made possible by sensitive and broadband instruments like *ASCA* and *BeppoSAX*, has triggered the need for time-dependent models describing the changes in particle spectra due to acceleration, energy losses, and diffusion. The problem is, in general, complex, and only some simplified cases have been treated up to now (e.g., Kirk, Rieger, & Mastichiadis 1998; Dermer 1998; Makino 1999). In addition, light travel time effects through the emitting region may be important (Chiaberge & Ghisellini 1999).

A crucial point in this problem is the measurement and interpretation of lags of the soft photons with respect to the harder ones. These can be produced through radiative cooling if the population of injected (accelerated) electrons has a low-energy cutoff or possibly a sharp low-energy break, as clearly shown by Kazanas, Titarchuk, & Hua (1998). If so, the observed lag $\tau_{\rm obs}$ depends only on the value of the magnetic field (assuming synchrotron losses are dominant, as is roughly the case for this source) and δ. Their relation can be expressed as

$$\boldsymbol{B}\delta^{1/3} \simeq 300\left(\frac{1+z}{\nu_1}\right)^{1/3}\left[\frac{1-(\nu_1/\nu_0)^{1/2}}{\tau_{\rm obs}}\right]^{2/3} \text{G}\,, \qquad (1)$$

where ν_1 and ν_0 represent the frequencies (in units of 10^{17} Hz) at which the observed lag (in seconds) has been measured.

It is interesting to note that the value of the lag (0.5 hr) inferred from the present *BeppoSAX* observations yield a $\boldsymbol{B}$ and δ combination consistent with the parameters obtained *independently* from the spectral fitting. This argument supports the radiative interpretation of the observed X-ray variability. An alternative possibility recently put forward by Dermer (1998) is that the flare decay is due to deceleration of the emitting plasma by entrainment of external matter as proposed for gamma-ray bursts. A detailed model would be needed for a quantitative comparison with the present data.

We recall that also in Mrk 421, a source closely similar to PKS 2155−304 in the SED, similar values of the lag have been found (Takahashi et al. 1996). In fact, the same arguments applied here to PKS 2155−304 give a similar estimate of the physical parameters for Mrk 421 (see Tavecchio et al. 1998). In the case of the other well-established TeV source, Mrk 501 lags have not been measured up to now.

7. SUMMARY AND CONCLUSIONS

Simultaneous multiwavelength monitoring has proved to be a very powerful tool to test and constrain emission models for blazars. The *BeppoSAX* observations of PKS 2155−304 reported here were partially overlapping with an intense gamma-ray flare detected by EGRET and with observations at TeV energies by the Mark 6 telescope, which also revealed a high flux.

Although exactly simultaneous gamma-ray data are not available at the time of writing, the X-ray data alone already provide us with interesting results. The X-ray flux was almost at the highest level ever detected. A curved spectral component, which can be identified with the high-energy end of the synchrotron emission, extends up to about 50 keV, while at higher energies the spectrum flattens, plausibly revealing the contribution of inverse Compton emission.

Indeed, this is what is generally expected in the context of emission from a relativistic jet, which seems quite convincingly to account for the SED of blazars. Within the blazar class, the synchrotron and inverse Compton components of low-power BL Lac objects, as is the case for PKS 2155−304, tend to peak at the highest energies (X-ray and TeV energies, respectively), and the synchrotron photons probably dominate the seed radiation field to be upscattered to gamma-ray energies.

Further constraints on the structure and physical parameters of the emitting source come from adding to the spectral the temporal information. Indeed, we find that SSC emission from a homogeneous region can consistently account for both the broadband SED and the soft lag detected by *BeppoSAX*, the latter being due to radiative cooling of the high-energy part of the electron distribution.

An interesting and testable prediction of this interpretation is the emission of TeV photons, which has been found a posteriori to be in remarkably good agreement with the results recently reported by the Mark 6 team (Chadwick et al. 1999).

We thank L. Piro, *BeppoSAX* Mission Scientist, and the chairman and members of the *BeppoSAX* Time Allocation Committee for allowing us to perform this observation in replacement of another target allocated to us, and the Mission Planning team at *BeppoSAX* SDC for the prompt scheduling. We also gratefully acknowledge conversations with D. Dal Fiume for extremely useful hints on PDS data reduction, and some suggestions by A. Santangelo about HPGSPC data reduction. A. C. and G. F. thank the Italian MURST for financial support.

REFERENCES

Boella, G., Butler, R. C., Perola, G. C., Piro, L., Scarsi, L., & Bleeker, J. A. M. 1997a, A&AS, 122, 299
Boella, G., et al. 1997b, A&AS, 122, 327
Brinkmann, W., et al. 1994, A&A, 288, 433
Canizares, C. R., & Kruper, J. 1984, ApJ, 278, L99
Chadwick, P. M., et al. 1999, ApJ, 513, 161
Chiaberge, M., & Ghisellini, G. 1999, MNRAS, in press
Chiappetti, L., Cusumano, G., Del Sordo, S., Maccarone, M. C., Mineo, T., & Molendi, S. 1998, Nucl. Phys. B, 69, 610
Chiappetti, L., & Dal Fiume, D. 1997, in Proc. of the 5th Workshop, Data Analysis in Astronomy, ed. V. Di Gesú et al. (Singapore: World Scientific), 101
Chiappetti, L., & Torroni, V. 1997, IAU Circ. 6776, 2
Courvoisier, T. J.-L., et al. 1995, ApJ, 438, 108
Cusumano, G., et al. 1999, Intercalibration of the *BeppoSAX* Narrow Field Instruments with Crab Nebula, in preparation
Dermer, C. D. 1998, ApJ, 501, L157
Dermer, C. D., Sturner, S. J., & Schlickeiser, R. 1997, ApJS, 109, 103
Edelson, R., et al. 1995, ApJ, 438, 120
Edelson, R. A., & Krolik, J. H. 1988, ApJ, 333, 646
Edelson, R., Pike, G. F., Saken, J. M., Kinney, A., & Shull, J. M. 1992, ApJS, 83, 1
Fossati, G., et al. 1998, Nucl. Phys. B, 69, 423
Frontera, F., Costa, E., Dal Fiume, D., Feroci, M., Nicastro, L., Orlandini, M., Palazzi, E., & Zavattini, G. 1997, A&AS, 122, 357
Giommi, P., et al. 1998, A&A, 333, L5
Hufnagel, B. R., & Bregman, J. N. 1992, ApJ, 386, 473
Kazanas, D., Titarchuk, L. G., & Hua, X.-M. 1998, ApJ, 493, 708
Kirk, J. G., Rieger, F. M., & Mastichiadis, A. 1998, A&A, 333, 452
Lockman, F. J., & Savage, B. D. 1995, ApJS, 97, 1
Madejski, G. M., Mushotzky, R. F., Weaver, K. A., Arnaud, K. A., & Urry, C. M. 1991, ApJ, 370, 198
Makino, F. 1999, in ASP Conf. Ser. 159, BL Lac Phenomenon, ed. L. O. Takalo & A. Sillanpää (San Francisco: ASP), in press
Makino, F., et al. 1996, in MPE Report 263, 413
Malkan, M. A., & Stecker, F. W. 1998, ApJ, 496, 13
Manzo, G., Giarrusso, S., Santangelo, A., Ciralli, F., Fazio, G., Piraino, S., & Segreto, A. 1997, A&AS, 122, 341
Padovani, P., & Giommi, P. 1995, ApJ, 444, 567
Parmar, A. N., et al. 1997, A&AS, 122, 309
Pesce, J. E., et al. 1997, ApJ, 486, 770
Pian, E., et al. 1997, ApJ, 486, 784
———. 1998, ApJ, 492, L17
Sreekumar, P., & Vestrand, W. T. 1997, IAU Circ., 6774, 2
Stecker, F. W., & de Jager, O. C. 1998, A&A, 334, L85
Takahashi, T., et al. 1996, ApJ, 470, L89
Tavecchio, F., Maraschi, L., & Ghisellini, G. 1998, ApJ, 509, 608
Treves, A., et al. 1998, ASP Conf. Ser. 159, BL Lac Phenomenon, ed. L. O. Takalo & A. Sillanpää (San Francisco: ASP), in press
Ulrich, M.-H., Maraschi, L., & Urry, C. M. 1997, ARA&A, 35, 445
Urry, C. M., et al. 1993, ApJ, 411, 614
———. 1997, ApJ, 486, 799
Urry, C. M., & Padovani, P. 1995, PASP, 107, 803
Vestrand, W. T., Stacy, J. G., & Sreekumar, P. 1995, ApJ, 454, L93
Zhang, Y. H., et al. 1999, ApJ, submitted